PALAEO 3

Re-evaluation and extension of the Marine Isotope Stage 5 tephrostratigraphy of the Faroe Islands region: The cryptotephra record

CrossMark

P.M. Abbott [a],*, W.E.N. Austin [b], S.M. Davies [a], N.J.G. Pearce [c], T.L. Rasmussen [d], S. Wastegård [e], J. Brendryen [f,g]

[a] Department of Geography, College of Science, Swansea University, Singleton Park, Swansea SA2 8PP, UK
[b] School of Geography and Geosciences, University of St. Andrews, North Street, St. Andrews KY16 9AL, UK
[c] Institute of Geography and Earth Sciences, Aberystwyth University, Llandinam Building, Penglais Campus, Aberystwyth SY23 3DB, UK
[d] Department of Geology, University of Tromsø, N-9037 Tromsø, Norway
[e] Department of Physical Geography and Quaternary Geology, Stockholm University, SE-10691 Stockholm, Sweden
[f] Department of Earth Science, University of Bergen, Post Box 7803, N-5007 Bergen, Norway
[g] Bjerknes Centre for Climate Research, Bergen, Norway

ABSTRACT

Previous studies of marine sequences from the Faroe Islands region have identified a series of coarse-grained tephra horizons deposited during Marine Isotope Stage (MIS) 5. Here we reassess the MIS 5 tephrostratigraphy of the Faroe Islands region and focus on the cryptotephra deposits preserved within the fine-grained fraction of marine core LINK 16. We also extend the record to encompass the late MIS 6 and early MIS 4 periods. A density separation technique, commonly used for tephra investigations in lacustrine settings but rarely applied to marine sediments, is utilised to explore the fine-grained material and EPMA and LA-ICP-MS are employed to determine the major and trace element composition of individual tephra shards. In total, 3 basaltic and 3 rhyolitic Icelandic cryptotephra deposits with homogeneous geochemical compositions are identified — all of which have the potential to act as isochronous tie-lines. Geochemical results highlight that the Grímsvötn volcanic system of Iceland is the predominant source of the basaltic horizons and the Öraefajökull or Torfajökull systems are the likely sources of the rhyolitic deposits. Three of the horizons have been previously recognised in Faroe Islands region marine sequences, with two of these deposits traceable into a Norwegian Sea sequence. An early MIS 4 rhyolitic horizon is the most widespread deposit as it can be traced into the Norwegian Sea and to the south into a record from the Rockall Trough. Basaltic and rhyolitic horizons deposited during late MIS 6 have not been recognised in other sequences and represent new additions to the regional tephrostratigraphy.

1. Introduction

1.1. Tephrochronology and the synchronisation of palaeoclimatic sequences

Tephrochronology provides a powerful technique for the correlation and synchronisation of palaeoclimatic sequences through the tracing of common volcanic ash horizons that represent isochronous tie-lines. This is especially valuable for marine sequences that fall beyond the radiocarbon window as independent time-scales cannot be constructed (Austin and Hibbert, 2012). Moreover, tephras have the potential to resolve the relative timing of rapid atmospheric and oceanic climate changes preserved within ice and marine cores. During Marine Isotope Stages (MIS) 6–4 significant climatic re-organisations occurred in association with the transitions into and out of the last interglacial period (MIS 5e, Eemian). In addition, there is increasing evidence that pronounced millennial-scale, climatic changes occurred during this period of changing climatic boundary conditions (e.g. Oppo et al., 1997; Rasmussen et al., 1999; Oppo et al., 2001; McManus et al., 2002; North Greenland Ice Core Project Members, 2004; Capron et al., 2010). New tephrostratigraphical frameworks for the Greenland ice-cores (e.g. Abbott et al., 2012) and existing frameworks for the marine realm (e.g. Fronval et al., 1998; Wastegård and Rasmussen, 2001; Brendryen et al., 2010; Abbott et al., 2013; Table 1) demonstrate the considerable potential of utilising tephrochronology as a correlation tool for the synchronisation of marine and ice-core sequences spanning MIS 6–4 (see Davies et al., in press). To date, however, very few studies have utilised a density separation technique, commonly applied to mineral-rich lacustrine sediments, to extract cryptotephra deposits from marine deposits. Here we apply this technique to isolate fine-grained tephra deposits within a marine core from the Faroe Islands region. LINK 16 has a high temporal resolution record for MIS 6–4 and we re-evaluate and extend the Faroe Islands tephrostratigraphy outlined in Wastegård and Rasmussen (2001). In addition we assess

* Corresponding author. Tel.: +44 1792 604138.
  E-mail address: p.abbott@swansea.ac.uk (P.M. Abbott).

Table 1
Summary of MIS 6–4 tephra horizons previously identified within marine sequences from the North Atlantic. T = Horizons with an affinity to the tholeiitic rock suite of Iceland. TA = Horizons with an affinity to the transitional alkali rock suite of Iceland. All horizons sourced from Iceland apart from 5d-DO26s/TRACHY-I sourced from Jan Mayen. Core locations are shown in Fig. 1. References: (1) Brendryen et al. (2010) (2) Abbott et al. (2011) (3) Wastegård and Rasmussen (2001) (4) Abbott et al. (2013) (5) Sjøholm et al. (1991) (6) Fronval et al. (1998) (7) Sejrup et al. (1989) (8) Lacasse and Garbe-Schönberg (2001).

Tephra name	Timing (MIS)	Composition	Core(s)	Location(s)	Ref.
4-DO19s/RHY-I, MD04-2822 2327–2328 cm	4	Rhyolitic (TA)	MD99-2289, MD04-2822	Norwegian Sea, Rockall Trough	1, 2
4-DO19i/BAS-I	4	Basaltic (T)	MD99-2289	Norwegian Sea	1
MD04-2822 2359–2366 cm	5a	Rhyolitic (T)	MD04-2822	Rockall Trough	2
5a-Top/BAS-I, 5a-DO21i/BAS-I, II, III	5a	Basaltic (T)	MD95-2009, MD99-2289	SE Norwegian Sea, Norwegian Sea	3, 1
MD04-2822 2385–2386 cm	5a	Rhyolitic (TA)	MD04-2822	Rockall Trough	4
5a-Low/BAS-I	5a	Basaltic (T)	MD95-2009	SE Norwegian Sea	3
5b-DO23s/BAS-I	5b	Basaltic (T)	MD99-2289	Norwegian Sea	1
MD04-2822 2424–2425 cm	5c	Rhyolitic (TA)	MD04-2822	Rockall Trough	4
5c-DO23i/BAS-I	5c	Basaltic (T)	MD99-2289	Norwegian Sea	1
5c-Midt/BAS-I, 5c-DO24s/BAS-I	5c	Basaltic (T)	MD95-2009, MD99-2289	SE Norwegian Sea, Norwegian Sea	3, 1
5d-Low/RHY-I, II, III, 5d-DO25i/RHY-I	5d	Rhyolitic (TA)	ENAM33, MD99-2289	NE Atlantic, Norwegian Sea	3, 1
MD04-2822 2490–2491 cm	5d	Rhyolitic (TA)	MD04-2822	Rockall Trough	4
5d-DO26s/TRACHY-I	5d	Trachybasalt	MD99-2289	Norwegian Sea	1
5e-Top/RHY	5e	Rhyolitic	ENAM33	NE Atlantic	3
5e-Top/BAS	5e	Basaltic	ENAM33	NE Atlantic	3
5e-Midt/RHY (5e-Eem/RHY-I)	5e	Rhyolitic (T)	ENAM33, MD99-2289, HM57-7, HM71-19, HM79-31, ODP 644, ODP 907	NE Atlantic, Norwegian Sea, Nordic Seas, Iceland Sea	3, 1, 5, 6, 7, 8
5e-Eem/TAB-I	5e	Basaltic (TA)	MD99-2289	Norwegian Sea	1
5e-Low/BAS-IV	5e	Basaltic (T)	ENAM33 MD95-2009	NE Atlantic SE Norwegian Sea	3

which tephra horizons are most valuable as isochronous markers and provide trace element characterisations of all identified horizons.

1.2. MIS 5 tephrostratigraphy of the Faroe Islands region

Previous studies of North Atlantic marine cores covering MIS 5 have identified tephra horizons and ash zones within the coarse sediment fraction (>150 μm diameter) (e.g. Sejrup et al., 1989; Sjøholm et al., 1991; Fronval et al., 1998; Wastegård and Rasmussen, 2001; Table 1), which may result in a bias towards the identification of iceberg-rafted and sea-ice rafted material (see Section 1.3). However, recent studies such as Brendryen et al. (2010) and Abbott et al. (2011, 2013) have demonstrated the potential to identify additional horizons if finer-sediment fractions (down to 25 μm diameter) are inspected for tephra content. This work has considerably increased the number of horizons that could act as isochronous tie-lines between MIS 5 North Atlantic marine sequences and the Greenland ice-core records.

Wastegård and Rasmussen (2001) identified a series of coarse-grained tephra horizons across the sub-stages of MIS 5 within two cores from the Faroe Islands region (Table 1). Six basaltic and 3 rhyolitic horizons were identified with a basaltic horizon at the base of MIS 5e traced between the cores. The most widespread tephra horizon during this period, the 5e-Midt/RHY first identified in the Nordic Seas (e.g. Sjøholm et al., 1991; Fronval and Jansen, 1997; Fronval et al., 1998; Haflidason et al., 2000; Lacasse and Garbe-Schönberg, 2001), was identified in MD95-2009 by Wastegård and Rasmussen (2001) and was subsequently traced into the Klaksvík terrestrial sequence on the Faroe Islands (Wastegård et al., 2005) and into the Norwegian Sea by Brendryen et al. (2010) (Fig. 1). A number of other horizons identified by Wastegård and Rasmussen (2001) have subsequently been traced within other marine records, for example Brendryen et al. (2010) suggested that the 5a-Top/BAS-I, 5c-Midt/BAS-I and 5d-Low/RHY-II deposits can be correlated to horizons in the Norwegian Sea (Table 1).

1.3. Challenges of utilising tephrochronology in the marine environment

One of the key principles of tephrochronology is that individual tephra horizons were deposited coevally in all sequences and that their stratigraphic position in different sequences is representative of the time of the eruption. However, within the marine environment a range of processes operate that can affect the transportation and deposition of material and thus, in some instances, impart temporal delays and affect the stratigraphic integrity of horizons.

As discussed by Brendryen et al. (2010, 2011) and Abbott et al. (2011) a consideration of transport processes is especially important in the high-northern latitudes of the Atlantic Ocean due to the potential operation of three transport pathways: primary airfall, sea-ice rafting and iceberg rafting. Primary airfall deposits are the most suitable deposits to act as chronostratigraphic markers and these typically display a homogenous chemical composition and are composed of fine-grained shards with a well-sorted size distribution (Abbott et al., 2011; Gudmundsdóttir et al., 2011). Sea-ice rafted deposits are characterised by similar features, however, tephra shards transported by this mechanism tend to be larger than those dispersed solely by atmospheric processes. Iceberg-rafted deposits are typically characterised by a heterogeneous geochemical composition and poor-size sorting (Brendryen et al, 2010; Abbott et al., 2011; Kuhs et al., 2014). These features are thought to result from the retention and amalgamation of tephra shards from a number of different eruptions within ice-sheets prior to the calving of icebergs and subsequent transport to the depositional site (Brendryen et al., 2010, 2011). Pinpointing iceberg-rafted deposits is crucial as this process can delay the deposition of material by centuries to millennia, and while they could be utilised in local core correlations they are inappropriate for the correlation of disparate sequences (Brendryen et al., 2010). Sea-ice rafted deposits are also prone to delayed deposition, however the potential lag of months to years is less than can be resolved in most marine sequences. As such, they can still be utilised for correlating widely-spaced records (Austin et al., 2004; Brendryen et al., 2010).

Secondary depositional processes, e.g. bioturbation, bottom-current reworking and mass movements, such as gravity induced sediment flows can affect tephra in the marine environment (Brendryen et al., 2010; Abbott et al., 2011; Todd et al., 2014). All of these processes can affect the vertical distribution of shards within a sequence and hamper the definition of the position of isochrons. This can occur either through the upward or downward movement of shards within the sediment column or prolonged delivery of material through redeposition in overlying sediments at the core site.

To assess the integrity of marine cryptotephra deposits, we undertook a systematic high-resolution down-core investigation of the different grain-size fractions to pinpoint distinct cryptotephra peaks relative to background shard levels along with a comprehensive geochemical characterisation of each horizon. Gudmundsdóttir et al. (2011) identified these as key factors for isolating tephra layers in the marine environment
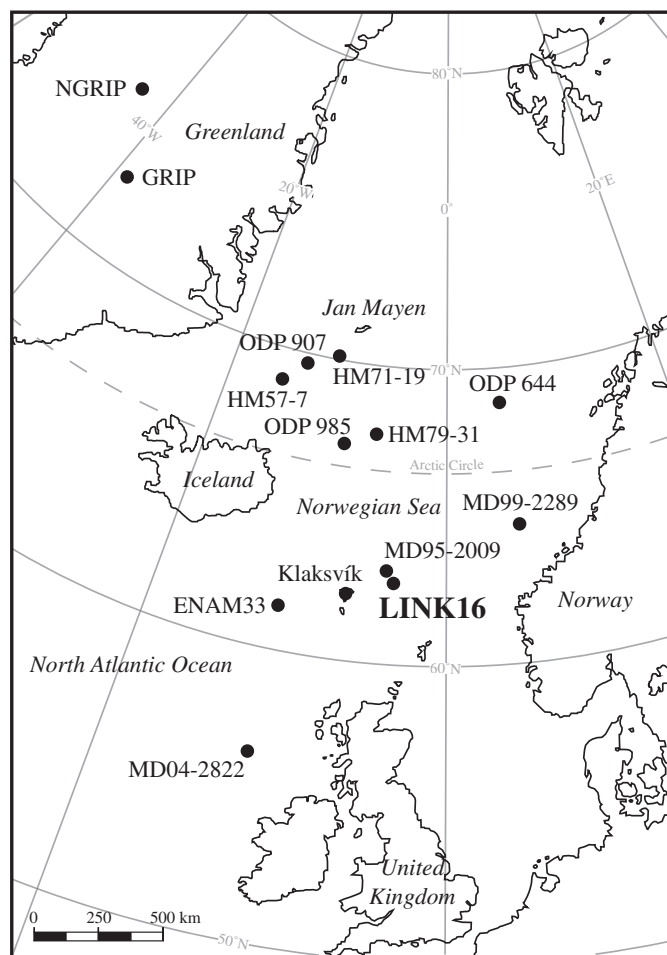
Fig. 1. Location map of the drilling sites for LINK 16 and other North Atlantic cores preserving MIS 6–4 tephra horizons.

and assessing if deposits were primary or reworked through the study of sequences proximal to Iceland. A stepped protocol for the assessment of marine tephra deposits and depositional transport pathways in glacial age distal sequences is outlined in Griggs et al. (in press).

2. Materials and methods

2.1. LINK 16

The LINK 16 core was retrieved from a water depth of 773 m from the Fugloyar Ridge, northeast of the Faeroe–Shetland Channel during a cruise of the RV Dana in August 2000 (62°36′N 3°31′W; Nielsen et al., 2007; Rasmussen and Thomsen, 2009). The period of interest for this study is between 420 and 800 cm depth as this relates to MIS 6–4 (Fig. 2).

The last interglacial period, MIS 5e, can be identified by low percentage abundance of the polar foraminiferal species *Neogloboquadrina pachyderma* (sinistral) preserved at the LINK 16 core site. Between ~660 and 700 cm depth this species drops dramatically while throughout the rest of the period it consistently exceeds 90% (Fig. 2ii; Rasmussen, unpublished; see also Rasmussen et al., 1999). This indicates that during the peak warmth of the interglacial the polar front migrated north over the core site, but was consistently south of the core site throughout the remainder of the study period. The substages of MIS 5 can be identified within the total number of planktonic foraminifera record, with high numbers deposited during the warm substages (5a, 5c, 5e) and low numbers during the cold substages (5b and 5d) (Fig. 2iii; Rasmussen et al., 1999). Akin to previous studies of cores from the region, peaks in the magnetic susceptibility record have been correlated to the North

Atlantic Dansgaard–Oeschger (DO) events that relate to the warm Greenland Interstadial (GI) events recorded in the Greenland ice-core records (Fig. 2i; e.g. Rasmussen et al., 1996; North Greenland Ice Core Project Members, 2004). The reduction in magnetic susceptibility during the MIS 5e warm period may result from dilution of the magnetic minerals by carbonate (Brendryen et al., 2010). The percentage abundance of grains larger than 100 μm in diameter can act as a proxy for ice-rafting at this site and Fig. 2v shows that ice-rafting at the site peaked during MIS 6, which coincides with the maximal ice-sheet extent during the MIS 6–4 period (Rasmussen, unpublished). Ice-rafting was variable throughout MIS 5 but general increases occurred at the transitions to the warm substages of MIS 5.

2.2. Identification of tephra shards in marine sediments

Sediment samples were initially investigated for tephra content at a low 5 cm contiguous resolution to ensure that all of the core sequence was inspected. Distinct peaks in shard concentration and peaks with similar stratigraphic contexts to previously identified horizons were reassessed at a higher 1 cm resolution. Samples were selected and prepared for geochemical analysis based on concentration profiles shown in Fig. 2iv. Tephra shards were isolated from the host sediment using a procedure modified from those outlined in Turney (1998), Davies et al. (2005) and Blockley et al. (2005) and previously applied to the study of marine sediments by Abbott et al. (2011, 2013). The samples were freeze dried and 0.5 g of dry weight sediment (gdw) was processed for tephra investigation. Carbonate material was removed through immersion overnight in dilute (10%) hydrochloric acid before the sediment was sieved into the grain-size fractions of >125, 80–125 and 25–80 μm and material <25 μm in diameter was discarded. The 25–80 μm grain-size fraction was then separated using sodium polytungstate at specific densities of 2.3 g/cm^3 (to remove biogenic material <2.3 g/cm^3) and 2.5 g/cm^3 (to isolate glass shards of rhyolitic composition 2.3–2.5 g/cm^3). Material with a density >2.5 g/cm^3 was retained to assess the presence of glass shards of basaltic composition. The >125 and 80–125 μm grain-size fractions and the material from the 25–80 μm fraction with densities between 2.3 and 2.5 g/cm^3 and >2.5 g/cm^3 were mounted in Canada Balsam for optical microscopic investigation. The same procedure was followed for samples selected for geochemical characterisation except material was mounted in epoxy resin on 28 by 48 mm microprobe slides to produce thin sections of individual shards for electron-probe micro-analysis (EPMA) and laser ablation inductively coupled plasma mass spectrometry (LA-ICP-MS). Sections were achieved by grinding and polishing the resin surfaces using silicon carbide paper and 6 and 1 μm diamond suspension, respectively.

2.3. Geochemical analysis of individual tephra shards

The major element composition of individual shards was determined by EPMA at the NERC Tephrochronological Analytical Unit, University of Edinburgh during two analytical periods. A Cameca SX100 electron microprobe with five vertical wavelength dispersive spectrometers was utilised using the operating conditions of Hayward (2012) summarised in Table 2. Calibration was achieved using pure metals, synthetic oxides and silicate standards. Secondary standards of Cannetto Lami Lava, Lipari (Periods 1 and 2), BHVO-2g (Period 1) and BCR2g (Period 2) were analysed at regular intervals to monitor for instrumental drift and to assess the precision and accuracy of analysed samples (Tables S1–3). For data comparison samples were normalised to an anhydrous basis (i.e. 100% total oxides), however, all the raw data values are provided in the supplementary information (Tables S5–S17).

Trace element characterisations of the individual shards were obtained using an LA-ICP-MS system at the Institute for Geography and Earth Sciences, Aberystwyth University during two analytical periods. This system couples a Coherent GeoLas 193 nm Excimer laser with a
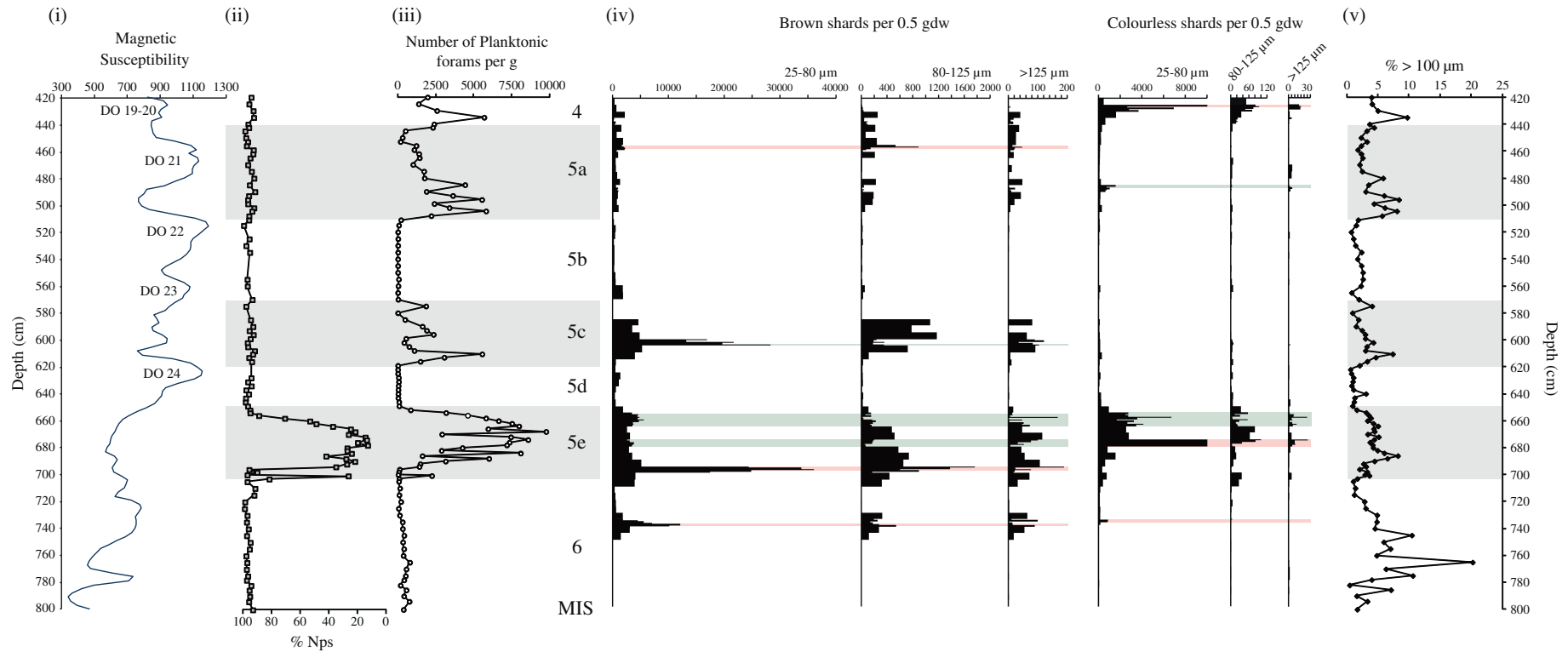
Fig. 2. Climate and tephrostratigraphy of the MIS 6–4 period within LINK 16. (i) Magnetic susceptibility, (ii) percentage abundance of *Neogloboquadrina pachyderma* (sinistral) (Rasmussen, unpublished), (iii) total number of planktonic forams per g of dry weight sediment (gdw) (Rasmussen, unpublished), (iv) tephrostratigraphy integrating 5 cm and 1 cm shard counts. Counts expressed as shards per 0.5 gdw. Red bars indicate tephra deposits defined as isochronous horizons. Green bars denote intervals of heterogeneous material or the analysis of additional material. (v) Percentage of grains larger than 100 μm (Rasmussen, unpublished).

Thermo Finnigan Element 2 high-resolution sector field mass spectrometer (Pearce et al., 2007, 2011). The operating conditions for this system are outlined in Table 2. Trace element concentrations were calculated using methods outlined in Pearce et al. (2007) with ^{29}Si, previously analysed for each shard during EPMA, utilised as the internal standard and the NIST 612 silicate glass used as the calibration standard. Analyses of reference glasses show that there is a consistent bias between determined and accepted concentrations due to fractionation effects, therefore a correction factor was applied to all analyses (see Pearce et al., 2011 for further details). Secondary standards analyses of BCR2g and BHVO-2g gained during the two analytical periods are provided in Table S4.

Geochemical heterogeneity is a key indicator of the operation of some processes in the marine environment, however, some heterogeneity in shard analyses can be introduced by the presence of crystal inclusions in the glass shards. As such, some outliers were discarded if trace element analyses indicated that the major element analyses were affected by the presence of microphenocryst/microlite inclusions (see Abbott et al., 2013 for further details) to prevent them from affecting the interpretation of depositional and transport processes.

3. Results

Fig. 2iv illustrates the tephrostratigraphy of LINK 16 and integrates the low-resolution shard counts (5 cm) with the high-resolution shard counts (1 cm) from selected sections. For most depth intervals major element analyses were obtained from shards in the 25–80 μm and >80 μm grain-size fractions, however, no distinct chemical differences between the two size ranges could be identified. Analyses from the different grain-size fractions were therefore grouped for data examination. All of the brown shards that were analysed were found to have a basaltic composition (Fig. 3bi) with affinities to the tholeiitic rock suite of Iceland. The colourless shards have a rhyolitic composition with compositional similarities to the Icelandic tholeiitic and transitional alkali rock suites (Fig. 3bii). In contrast to the findings of Abbott et al. (2012) and Brendryen et al. (2010) there is no evidence of material from the Jan Mayen volcanic system. The following sections describe the LINK 16 tephrostratigraphy, geochemical characterisations and potential transport processes responsible for tephra deposition within four climatic intervals. Potential correlations to tephra horizons in other MIS 6–4 palaeoclimatic sequences are also investigated.

3.1. MIS 6 deposits

Within the late MIS 6 period just prior to the transition into the MIS 5e period, peaks in both brown and clear tephra shards were identified at depths of 738–739 cm and 735–737 cm, respectively.

3.1.1. 738–739 cm

Major element analyses of brown shards from this peak, most apparent in the 25–80 μm grain-size fraction, demonstrate that the deposit has a homogeneous basaltic tholeiitic composition with SiO$_2$ values between 48.8 and 50.2 wt%, CaO values of ~10.1 wt%, FeO values of ~14.25 wt% and TiO$_2$ values between 3.08 and 3.5 wt% (Table 2). Comparison with material proximal to Icelandic tholeiitic systems demonstrates that this deposit has a Grímsvötn-like composition (Fig. 3c).

3.1.2. 735–737 cm

This colourless shard peak is only observed in the 25–80 μm fraction with a maximum shard count of 900 shards per 0.5 gdw. However, it does stand out from background tephra levels during this interval. Major element analyses show a homogenous rhyolitic deposit with an affinity to the Icelandic transitional alkali rock suite (Fig. 3bii). SiO$_2$ values range between 73.8 and 74.6 wt%, Al$_2$O$_3$ concentrations are ~12.5 wt%, FeO concentrations are between 2.75 and 3.42 wt% and the total alkalis range between 8.8 and 9.2 wt%. A comparison to proximal

Icelandic rhyolitic material suggests an origin from either the Öraefajokull or Torfajökull volcanic system (Fig. 3d).

Both horizons were deposited during a period of decreasing IRD levels following a period of unstable IRD deposition, possibly related to the advance and retreat of ice sheets during MIS 6 (Fig. 2v). Both horizons are not directly related to distinct peaks in IRD levels and the small grain-size of the material may indicate that deposition occurred through primary airfall processes. Wastegård and Rasmussen (2001) identified a small peak in basaltic grains within the MIS 6 section of the MD95-2009 core which may relate to LINK 16 738–739 cm, however, the material was not geochemically characterised. A potential late MIS 6 rhyolitic horizon (133 ka) which may correlate to LINK 16 735–737 cm was identified by Lacasse and Garbe-Schönberg (2001) in ODP 985 from the Norwegian Basin. However, as only average and standard deviation values were presented a direct geochemical comparison is not possible. Consequently, these horizons are considered to represent new marker horizons for the late MIS 6 period.

3.2. MIS 5e (Eemian) deposits

Throughout MIS 5e elevated levels of both brown and colourless tephra shards are observed (Fig. 2iv). Three core sections were investigated at high-resolution (695–700 cm, 675–680 cm and 655–665 cm), showing a very distinct brown shard peak between 695 and 698 cm and a colourless shard peak at 675–680 cm with shard counts in excess of 10,000 shards per 0.5 gdw in all five samples (Fig. 2iv). Background levels of shards were identified in the other sections. In addition to geochemically analysing material from the main peaks brown shards from the 675–680 cm interval and both brown and colourless shards from the 660–665 cm interval were analysed to assess whether the background shard levels throughout MIS 5e relate to the main peaks.

3.2.1. 695–698 cm

Shards from this peak have a relatively homogeneous composition with a dominant population of basaltic tholeiitic material (population a) (Fig. 3bi). This population has SiO$_2$ concentrations between 49.3 and 50.6 wt%, TiO$_2$ values of ~2.60 wt%, FeO concentrations of ~14.1 wt% and CaO values ranging between 9.7 and 10.3 wt% indicating strong affinities to the products of the Grímsvötn system (Fig. 3c). Glass shards with this affinity are also present at 675–680 cm and 660–665 cm depth, however, both have a significant sub-population with ~30% of shards characterised by higher TiO$_2$ compositions of ~3.1–3.3 wt% (population b; Fig. 4ai). Two (10%) of the shards analysed from the 695–698 cm horizon have affinities to population b (Fig. 4a).

Deposition of the LINK 16 695–698 cm horizon is not directly related to a peak in the IRD proxy (Fig. 2) and the prevalence of small tephra shards in this deposit suggests that LINK 16 695–698 cm can be regarded as an isochronous deposit most likely deposited via airfall processes. The overall profile of basaltic tephra within the MIS 5e period reveals a sharp lower contact, a distinct peak in shard concentrations and an upward tail of deposition. Glass shards of identical composition are observed at least 25 cm above the main peak. The upward tail could be due to the input of material from subsequent eruptions and/or the operation of secondary transport processes. The later may relate to bioturbation of material in the sediment column and resedimentation of tephra shards due to bottom current transport, which would be elevated due to increased bottom current speeds during MIS 5e, and contribute to the elevated background tephra shard counts and particles >100 μm deposited at the site. The geochemical evidence suggests that both scenarios are possible. The elevated dominance of population b in the 675–680 cm and 660–665 cm samples indicates the input of material from a subsequent volcanic eruption while the persistence of material related to the main population of 695–698 cm suggests that secondary transport processes were operating. However, as the peak in material between 695 and 698 cm is so high relative to the background levels

Table 2

Mean and 1σ standard deviation major, minor and trace element values for homogenous MIS 6–4 tephra horizons within the LINK 16 core with the potential to act as widespread isochrons. Total oxide values are raw values before normalisation. All major and minor elements are expressed as weight percentage and have been normalised to 100% total oxides. Trace elements expressed as parts per million (ppm). Total iron is expressed as FeO. n = number of shards analysed. EPMA operation conditions: Two sets of column conditions were utilised within the EPMA analysis. Firstly Na, Al, Si, K, Ca, Mg and Fe were determined using an accelerating voltage of 15 kV and a beam current of 2 nA. F, Cl, P, S, Ti and Mn were then determined using an accelerating voltage of 15 kV and a beam current of 80 nA. A 5 μm electron beam diameter was used throughout. Counting times were 20 s at the peak position and 10 s for background for all elements except F (50 s and 40 s), Ti (30 s and 15 s), Mn (50 s and 40 s) and Fe (40 s and 20 s). SO_2, F and Cl were not measured during analytical period 2. LA-ICP-MS Operating Conditions: For these analyses a laser beam diameter of 10 or 20 μm (depending on the size of shard sections) pulsed at a frequency of 5 Hz with a fluence of 10 J/cm^2 and a flash duration of ~10 ns was utilised. Analyses took ~30 s and argon was used as the carrier gas.

	LINK 16 425–427 cm	LINK 16 456–457 cm	LINK 16 675–680 cm	LINK 16 695–698 cm	LINK 16 735–737 cm	LINK 16 738–739 cm
n	10	27	8	14	12	14
SiO_2	74.86 (0.26)	49.74 (0.35)	77.47 (0.26)	50.18 (0.31)	74.26 (0.27)	49.73 (0.31)
TiO_2	0.15 (0.01)	3.09 (0.13)	0.21 (0.01)	2.60 (0.03)	0.23 (0.00)	3.17 (0.13)
Al_2O_3	13.06 (0.14)	13.05 (0.23)	11.43 (0.20)	13.48 (0.28)	12.52 (0.10)	13.01 (0.24)
FeO	2.16 (0.15)	14.55 (0.38)	3.06 (0.17)	14.08 (0.19)	3.14 (0.19)	14.26 (0.39)
MnO	0.07 (0.01)	0.25 (0.01)	0.10 (0.01)	0.24 (0.01)	0.11 (0.01)	0.24 (0.01)
MgO	0.08 (0.03)	5.52 (0.26)	0.02 (0.01)	5.46 (0.13)	0.01 (0.02)	5.71 (0.14)
CaO	0.75 (0.07)	10.36 (0.27)	1.56 (0.09)	10.11 (0.17)	0.74 (0.02)	10.08 (0.17)
Na_2O	4.75 (0.11)	2.73 (0.13)	4.26 (0.08)	2.83 (0.18)	4.94 (0.11)	2.76 (0.15)
K_2O	4.10 (0.12)	0.40 (0.04)	1.88 (0.08)	0.52 (0.04)	4.05 (0.08)	0.45 (0.02)
P_2O_5	0.01 (0.01)	0.30 (0.02)	0.01 (0.01)	0.26 (0.01)	0.01 (0.00)	0.33 (0.02)
SO_2	N/A	N/A	N/A	0.16 (0.04)	N/A	0.21 (0.04)
F	N/A	N/A	N/A	0.05 (0.01)	N/A	0.04 (0.01)
Cl	N/A	N/A	N/A	0.03 (0.00)	N/A	0.02 (0.00)
Total Oxides	96.03 (0.73)	98.31 (0.93)	95.65 (1.37)	98.90 (0.80)	95.70 (0.56)	98.72 (0.65)
Rb	81.24 (9.49)	7.38 (2.96)	28.85 (1.78)	11.17 (4.51)	65.49 (5.84)	6.21 (3.54)
Sr	39.77 (4.85)	175.90 (20.99)	59.46 (6.44)	237.53 (39.52)	31.14 (11.82)	199.24 (22.29)
Y	105.18 (15.95)	36.74 (6.32)	133.22 (14.26)	41.08 (6.22)	104.26 (12.22)	45.15 (8.24)
Zr	545.90 (49.19)	205.22 (33.51)	618.35 (44.98)	186.72 (40.62)	1096.53 (153.53)	196.23 (47.96)
Nb	90.55 (8.47)	18.76 (1.89)	81.94 (3.89)	21.04 (3.97)	182.97 (11.87)	19.80 (2.90)
Ba	909.06 (123.23)	86.23 (15.99)	358.36 (29.60)	110.57 (36.45)	680.55 (63.68)	90.92 (11.67)
La	95.93 (8.54)	14.58 (2.31)	73.87 (4.43)	16.87 (4.18)	140.40 (17.66)	16.98 (2.70)
Ce	202.95 (19.03)	34.07 (4.27)	151.72 (4.13)	37.84 (4.26)	261.16 (21.99)	37.71 (3.84)
Pr	22.68 (2.20)	5.07 (0.79)	18.96 (1.09)	5.76 (0.89)	30.38 (3.14)	5.14 (0.75)
Nd	87.44 (12.48)	23.09 (3.90)	77.38 (7.63)	26.68 (5.15)	111.62 (10.94)	25.24 (3.95)
Sm	17.32 (3.57)	6.33 (1.58)	17.95 (1.06)	8.23 (2.78)	22.11 (2.42)	7.84 (3.19)
Eu	2.36 (1.27)	2.46 (0.95)	3.33 (0.36)	2.05 (1.13)	3.81 (1.08)	2.55 (1.02)
Gd	15.20 (4.27)	5.57 (1.64)	15.38 (2.18)	7.05 (1.58)	16.76 (2.25)	8.33 (2.71)
Tb	3.22 (0.52)	1.18 (0.32)	3.52 (0.77)	1.34 (0.77)	3.46 (0.70)	1.19 (0.40)
Dy	15.95 (2.93)	7.44 (1.72)	22.17 (3.15)	7.16 (3.39)	20.34 (2.33)	9.92 (2.40)
Ho	3.09 (0.76)	1.30 (0.26)	4.68 (0.67)	1.58 (0.55)	3.71 (0.53)	1.85 (0.31)
Er	9.80 (2.04)	3.21 (0.84)	13.14 (0.76)	4.74 (2.00)	10.44 (1.10)	4.62 (1.08)
Tm	1.39 (0.33)	0.45 (0.22)	1.92 (0.35)	0.46 (0.59)	1.57 (0.33)	0.40 (0.60)
Yb	10.96 (1.94)	4.06 (0.60)	17.83 (1.53)	4.62 (1.30)	12.48 (1.73)	4.90 (1.58)
Lu	1.77 (0.44)	0.56 (0.16)	2.70 (0.37)	0.68 (0.67)	1.71 (0.38)	0.94 (0.59)
Hf	17.26 (2.79)	4.82 (1.03)	19.13 (3.23)	5.63 (1.65)	29.72 (4.84)	5.71 (1.08)
Ta	7.11 (1.14)	1.35 (0.24)	5.17 (0.48)	1.53 (0.41)	10.82 (1.05)	1.56 (0.82)
Pb	9.28 (1.55)	1.64 (0.78)	3.57 (0.52)	2.47 (1.13)	6.98 (1.11)	1.77 (0.58)
Th	16.85 (2.22)	1.34 (0.36)	8.57 (0.67)	2.02 (0.63)	18.85 (2.20)	1.77 (0.31)
U	3.77 (0.40)	0.38 (0.11)	2.01 (0.23)	0.54 (0.17)	4.34 (0.44)	0.58 (0.35)

the potential operation of these processes does not affect the use of this peak as the position of the isochronous horizon.

The basaltic shard concentration profile in LINK 16 throughout MIS 5e is akin to the one observed by Wastegård and Rasmussen (2001) within MD95-2009 and defined as the 5e-Low/BAS-IV horizon. This was traced into ENAM33, however in this record the shard profile does not have a clear shard peak but a wide zone of elevated concentrations, with the base defined as the 5e-Low/BAS-IV and shards from the top of this zone defined as 5e-Top/BAS. These horizons shows a strong compositional relationship to population a of the LINK 16 695–698 cm deposit (Fig. 4b). It is thus, highly likely that the large peak in basaltic material at 695–698 cm depth correlates to the 5e-Low/BAS-IV.

3.2.2. 675–680 cm

The colourless shards from this interval are rhyolitic in composition, with a dominant population with affinities to the tholeiitic rock suite of Iceland (Fig. 3bii). This material has SiO_2 concentrations between 77 and 77.9 wt%, Al_2O_3 values of ~11.4 wt%, FeO concentrations of ~3 wt% and CaO values between 1.4 and 1.65 wt%. A secondary population of three analyses is present, this material has lower CaO and SiO_2 concentrations, but higher K_2O and Al_2O_3 concentrations and is related to the transitional alkali rock suite of Iceland. Shards from the background levels between 655 and 665 cm have a composition similar to the main population of LINK 16 675–680 cm (Fig. 4c).

The main population of LINK 16 675–680 cm can be correlated to the widespread 5e-Midt/RHY (5e-Eem/RHY-I in Brendryen et al. (2010)) (Fig. 4c; Table 1). The presence of shards of the same composition as LINK 16 675–680 cm further up the sequence at 660–665 cm depth provides further supporting evidence for the operation of secondary transport processes, described earlier, during the MIS 5e period. However, the high shard counts, distinctness of the peak in concentration and lack of coincident peak in the IRD proxy suggests that LINK 16 675–680 cm can be regarded as an isochronous horizon.

3.3. MIS 5c deposit

There is a general increase in the number of brown tephra shards deposited during MIS 5c, which may result from increased bottom current resedimentation during this warm interval. However, a distinct peak in shards of all grain-sizes is observed in the low-resolution record of tephra content between 600 and 605 cm. Within high-resolution analyses a distinct peak was apparent within the 25–80 μm grain-size fraction, with the highest shard counts in the 604–605 cm sample (Fig. 2iv).

3.3.1. 604–605 cm

Brown tephra shards from this peak show affinities to the Icelandic tholeiitic rock suite, however, the overall composition of the deposit is heterogeneous, with three distinct populations apparent (Fig. 5a). The populations can be distinguished most clearly by differences in the TiO_2 concentrations of individual shards (Fig. 5ai). Population a has

affinities to material produced both by the Grímsvötn and Kverkfjöll systems, population b has a Grímsvötn-like composition and population c has the strongest affinity to material from the Kverkfjöll system (Fig. 5a).

The three clear geochemical populations of LINK 16 604–605 cm indicates that this deposit is composed of material from a number of

Fig. 3. (a) Total alkali versus silica plot for tephra deposits identified in LINK 16. (b) (i) Inset of the total alkali versus silica plot focusing on the basaltic material. Division line between alkaline and subalkaline (tholeiitic) material from MacDonald and Katsura (1964). (ii) Inset of the total alkali versus silica plot focusing on the rhyolitic material. Geochemical fields for the Icelandic rock suites derived from Jakobsson et al. (2008). Chemical classification and nomenclature on all plots after Le Maitre et al. (1989). (c) (i) K_2O vs. TiO_2 and (ii) CaO vs. FeO compositional variation diagrams comparing analyses from three homogenous tholeiitic basaltic LINK 16 horizons to characterisations of material proximal to four tholeiitic Icelandic volcanic systems. Geochemical fields defined using analyses from Jakobsson et al. (2008) (Reykjanes), Höskuldsson et al. (2006) and Óladóttir et al. (2011) (Kverkfjöll) and Jakobsson (1979), Haflidason et al. (2000) and Óladóttir et al. (2011) (Grímsvötn and Veidivötn-Bardabunga). (d) (i) CaO vs. FeO (ii) Al_2O_3 vs. Na_2O compositional variation diagrams comparing analyses from two homogenous transitional alkali rhyolitic LINK 16 horizons to characterisations of rhyolitic material proximal to four transitional alkali Icelandic volcanic systems. Geochemical fields defined using individual silicic rock analyses reported by Jónasson (2007, unpublished).
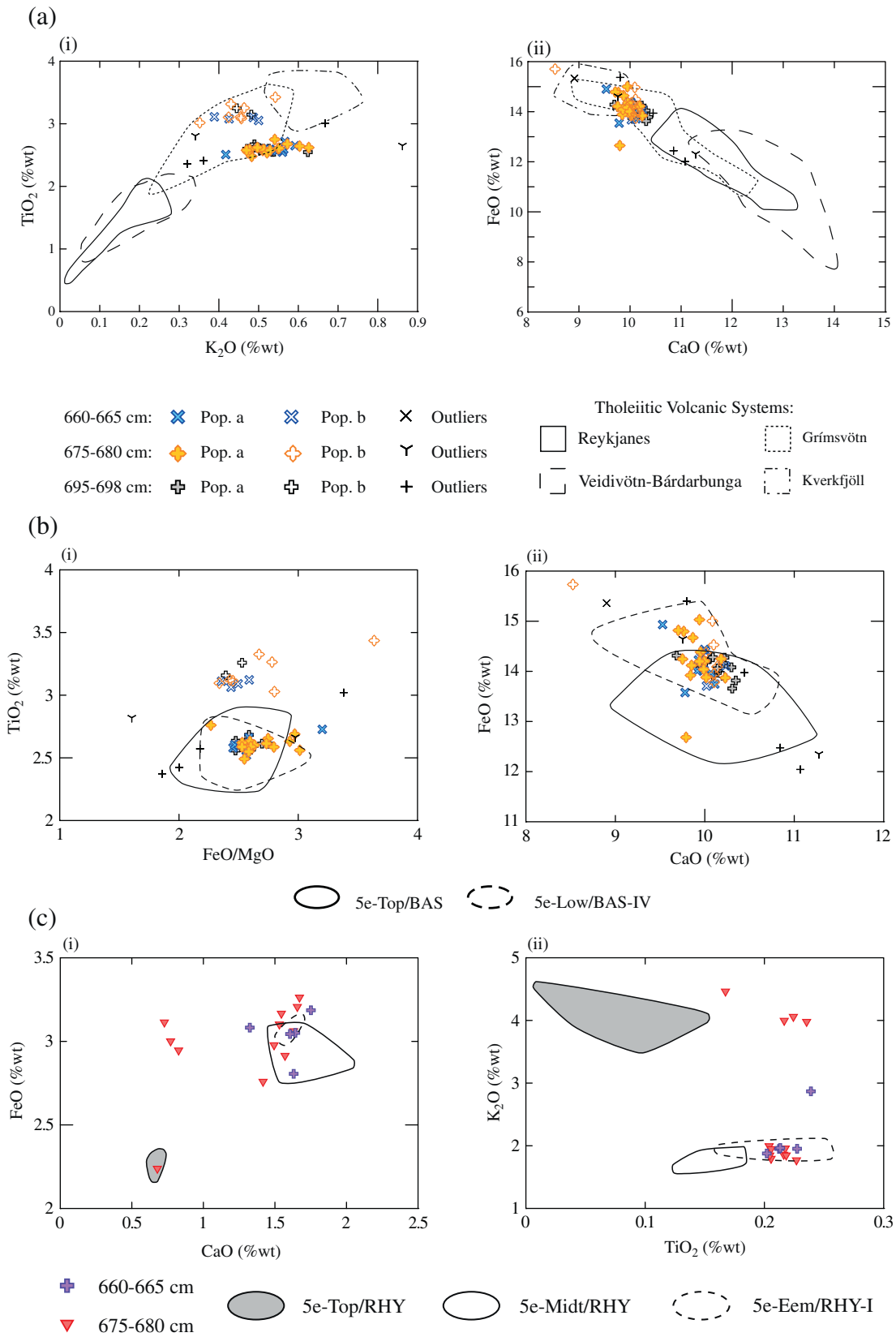
Fig. 4. (a) (i) K$_2$O vs. TiO$_2$ and (ii) CaO vs. FeO compositional variation diagrams comparing MIS 5e tholeiitic basaltic material to characterisations of material proximal to four tholeiitic Icelandic volcanic systems. Geochemical fields defined using analyses from Jakobsson et al. (2008) (Reykjanes), Höskuldsson et al. (2006) and Óladóttir et al. (2011) (Kverkfjöll) and Jakobsson (1979), Haflidason et al. (2000) and Óladóttir et al. (2011) (Grímsvötn and Veidivötn-Bardabunga). (b) Geochemical comparisons between MIS 5e basaltic material in LINK 16 and the 5e-Top/BAS and 5e-Low/BAS-IV horizons defined by Wastegård and Rasmussen (2001). (c) (i) CaO vs. FeO (ii) TiO$_2$ vs. K$_2$O compositional variation diagrams comparing rhyolitic material from 660–665 cm and 675–680 cm depth in LINK 16 to MIS 5e deposits identified in other sequences. 5e-Top/RHY and 5e-Midt/RHY from Wastegård and Rasmussen (2001) and 5e-Eem/RHY-I from Brendryen et al. (2010).

volcanic eruptions. The relatively discrete nature of the deposit and clear peak in shard deposition suggests a rapid input of material rather than the mixing of material from three closely-timed eruptions by bioturbation within the sediment column. Deposition via iceberg rafting can create such geochemical heterogeneity and a small peak in the IRD proxy can be observed around this depth. Fine-grained material (25–80 μm) dominates this deposit which may indicate that the glass shards were deposited onto an ice-sheet surface downwind from the eruption source prior to rafting.

Wastegård and Rasmussen (2001) identified a MIS 5c Grímsvötn sourced basaltic horizon, 5c-Midt/BAS-I, and Brendryen et al. (2010) subsequently correlated 5c-DO24s/BAS-I to this deposit (Table 1). In addition, Brendryen et al. (2010) identified another MIS 5c Grímsvötn-sourced horizon, 5c-DO23i/BAS-I, in the Norwegian Sea record. Fig. 5b demonstrates that the composition of population b of LINK 16 604–605 cm has strong compositional similarities to the 5c-Midt/BAS-I (5c-DO24s/BAS-I) horizon. However, neither of these latter horizons have any associated chemical sub-populations. The higher degree of heterogeneity within the LINK 16 deposit might be due to the analysis of significantly more shards within this study or that these sub-populations are only preserved in the fine-grained material analysed in this study.

Deposition of 5c-Midt/BAS-I and 5c-DO24s/BAS-I in the two cores can be directly related to spikes in IRD concentration (Rasmussen et al., 2003; Brendryen et al., 2010). In addition, LINK 16 604–605 cm falls in a stadial phase following a magnetic susceptibility peak thought to relate to DO-24, which is highly similar to the stratigraphic position of 5c-DO24s/BAS-I in MD99-2289 (Brendryen et al., 2010). Therefore, these horizons can be correlated as a regional marine–marine core tie-line for the middle of MIS 5c. However, the ice-rafted nature of this horizon may have significantly delayed deposition following the eruptive events preventing it from acting as an isochronous tie-line to more disparate palaeoclimatic records, specifically the Greenland ice-cores.

3.4. MIS 5a and 4 deposits

Based on the low-resolution shard counts four depth intervals from this period were re-assessed for high-resolution tephra content. Distinct peaks in colourless shards were identified between 485 and 486 cm and 425 and 427 cm and a peak in brown shards between 456 and 457 cm (Fig. 2iv).

3.4.1. 485–486 cm

High-resolution tephra counts show a peak in colourless shards 25–80 μm in diameter at this depth (Fig. 2iv). Shard concentrations are low compared to those observed in the MIS 5e period, but the peak is distinct from background levels during MIS 5a. Geochemical results display a heterogeneous composition with four sub-populations apparent within the overall characterisation (Fig. 3bii). The heterogeneity of this deposit indicates that it could have been deposited by iceberg rafting or resulted from mixing of material in the sediment column. Therefore, this deposit was not investigated further for use as an isochronous marker horizon.

3.4.2. 456–457 cm

A distinct peak of brown tephra shards in the 80–125 μm grain-size fraction with a shard concentration of ~900 shards per 0.5 gdw was observed at 456–457 cm. Geochemical analyses reveal a relatively homogenous composition with affinities to the Icelandic tholeiitic rock suite (Fig. 3bi). The individual shards have SiO_2 values ranging between 48.9 and 50.5 wt%, Al_2O_3 values of ~13 wt%, FeO concentrations between 13.9 and 15.3 wt% and Na_2O concentrations of ~2.7 wt% typical of Grímsvötn products (Table 2; Fig. 3c).

Wastegård and Rasmussen (2001) identified a distinct peak in basaltic material, 5a-Top/BAS-I, in a similar stratigraphic position at the top of MIS 5a in the MD95-2009 core. In MD99-2289 Brendryen et al. (2010) identified a zone of basaltic material at the top of MIS 5a with three distinct shard peaks (5a-DO21i/BAS-I, II and III). They are all geochemically homogenous, with indistinguishable major element fingerprints and all a potential match to the 5a-Top/BAS-I (Fig. 6a; Table 1). These three deposits have been interpreted as the products of three closely-timed eruptions (Brendryen et al., 2010). Shards from 5a-DO21i/BAS-I, II and III have been reanalysed to permit trace element comparisons (see Section 3.6; Table S16). The new major element analyses are used for comparisons to LINK 16 as they have been determined on the same microprobe under the same analytical conditions. Major element comparisons demonstrate similarities between LINK 16 456–457 cm and all three peaks in MD99-2289 (Fig. 6a). It is therefore not possible to suggest a specific correlation between LINK 16 and MD99-2289 and some subtle differences in average values will be discussed further in Section 3.6.1. The homogeneity of this deposit and deposition during a period of low IRD deposition suggests that the material was not deposited via iceberg rafting. The occurrence of the main peak in shards in the 80–125 μm grain-size fraction, without significant numbers in the 25–80 μm or >125 μm fractions, could indicate that the material was sea-ice rafted to the site or that the main atmospheric dispersal pathway was towards the LINK 16 site. Neither of these processes would impart a significant temporal delay on deposition, therefore, LINK 16 456–457 cm can be considered an isochronous marker horizon.

3.4.3. 425–427 cm

A distinct peak in colourless tephra shards is identified at 425–427 cm within all three grain-size fractions. Exceeding 10,000 shards per 0.5 gdw the peak in the 25–80 μm fraction falls 1 cm above the peaks in the coarser fractions (Fig. 2iv). This horizon has a homogenous transitional alkali rhyolitic composition (Fig. 3bii) with SiO_2 concentrations between 74.0 and 75.3 wt%, Al_2O_3 values of ~13.1 wt%, FeO concentrations ranging between 2.0 and 2.4 wt% and total alkali values between 8.6 and 9.5 wt% (Table 2). This horizon has affinities to material sourced from the Öraefajökull and Torfajökull volcanic systems (Fig. 3d).

LINK 16 425–427 cm occurs shortly after a peak in the IRD proxy (Fig. 2), however, the homogenous composition of the material and the small shard size within this deposit suggests that the material was deposited via primary airfall and represents an isochronous horizon. It was deposited during the early part of MIS 4 close to the transition from MIS 5a (Fig. 2). Two rhyolitic horizons of a similar age and composition have been identified in other North Atlantic marine records (Fig. 7). Abbott et al. (2011) identified MD04-2822 2327–2328 cm within the MIS 4 section of a Rockall Trough core and Brendryen et al. (2010) described the identification of the 4-DO19s/RHY-I horizon in the Norwegian Sea (Table 1). Abbott et al. (2011) previously explored the potential correlation of one population of MD04-2822 2327–2328 cm to the 4-DO19s/RHY-I, but ruled out a link based on slight geochemical offsets between the deposits (see Fig. 7 of Abbott et al., 2011). Reanalysis of shards from 4-DO19s/RHY-I on the same microprobe and operating conditions as the MD04-2822 and LINK 16 horizons strongly indicates that the three horizons relate to the same volcanic event and can be used as an isochronous tie-line between the records (Fig. 7a). Brendryen et al. (2010) and Owen et al. (2013) propose that this eruption could relate to an event that produced two tuyas in the Torfajökull area of Iceland dated by Ar/Ar to 67 ± 9 and 72 ± 7 ka BP (McGarvie et al., 2006). This dating is comparable to the ages of 70.1 ka BP and 68.45 ± 1.5 ka BP assigned to the marine occurrences by Brendryen et al. (2010) and Abbott et al. (2013) respectively. Geochemical comparisons between proximal and distal material by Brendryen et al. (2010) and Abbott et al. (2013) did not directly support a match, however, this may relate to the use of different analytical techniques to geochemically characterise the proximal and distal material.
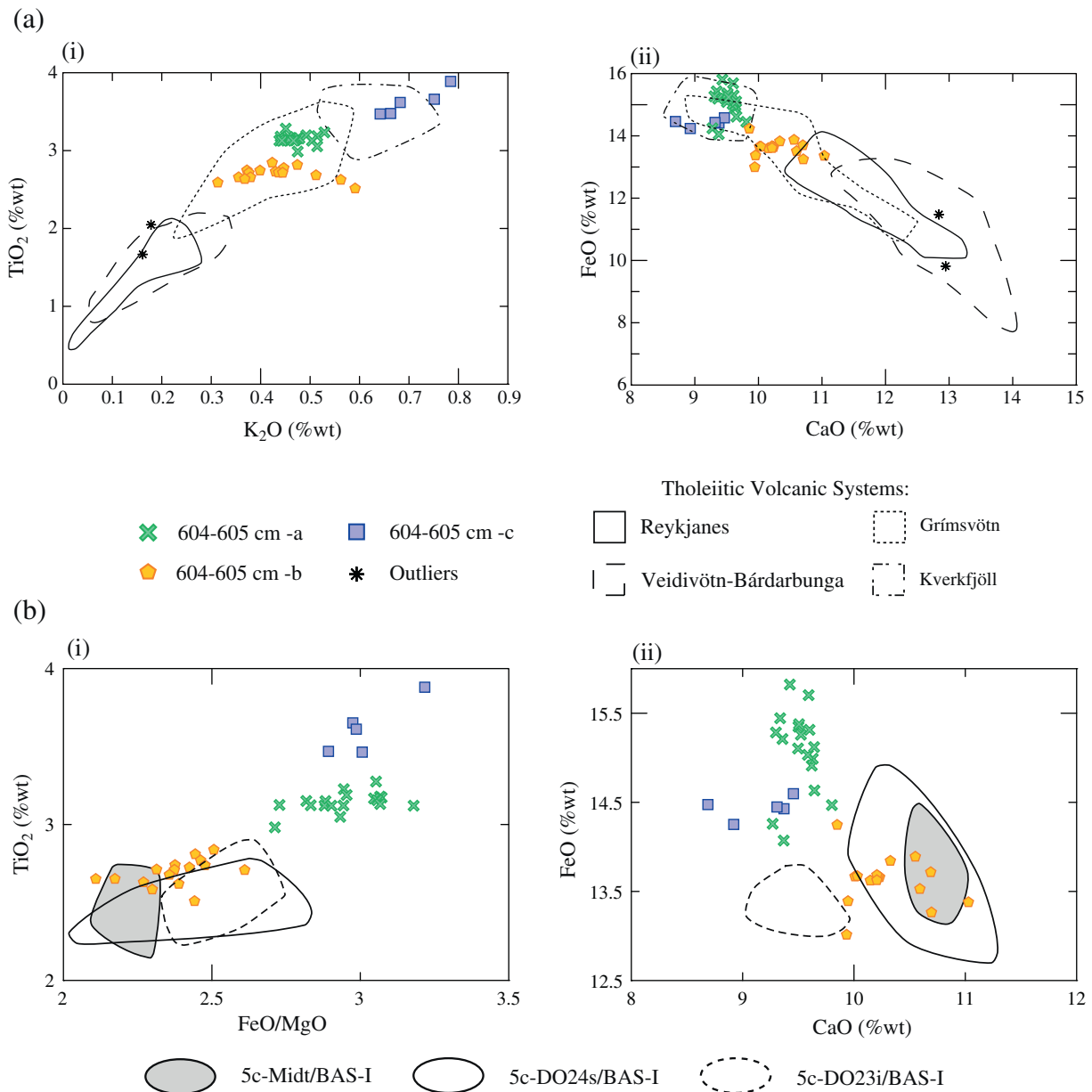
Fig. 5. (a) (i) K₂O vs. TiO₂ and (ii) CaO vs. FeO compositional variation diagrams comparing material from 604–605 cm depth in LINK 16 to characterisations of material proximal to four tholeiitic Icelandic volcanic systems. Geochemical fields defined using analyses from Jakobsson et al. (2008) (Reykjanes), Höskuldsson et al. (2006) and Óladóttir et al. (2011) (Kverkfjöll) and Jakobsson (1979), Haflidason et al. (2000) and Óladóttir et al. (2011) (Grímsvötn and Veidivötn-Bardabunga). (b) Comparison on the composition of three geochemical populations within LINK 16 604–605 cm to MIS 5c tephra horizons identified in other North Atlantic sequences. 5c-Midt/BAS-I from Wastegård and Rasmussen (2001) and 5c-DO24s/BAS-I and 5c-DO23i/BAS-I from Brendryen et al. (2010).

3.5. Trace element characterisation of tephra horizons

Glass shards from all deposits described above were analysed for their trace element composition to provide a secondary fingerprint and to help test two proposed correlations. In the two deposits with a heterogeneous major element composition (LINK 16 485–486 cm and 604–605 cm) heterogeneity was also observed in the trace element characterisations and the trace element populations are consistent with those defined by major element analysis (see Supplementary Information). For the deposits classified as isochronous marker horizons (LINK 16 425–426 cm, 456–457 cm, 675–680 cm, 695–697 cm, 735–737 cm and 738–739 cm) rare earth element (REE) profiles demonstrate the relative homogeneity of the trace element characterisations providing a secondary geochemical fingerprint for each horizon (Fig. 8a and b). An increase in variability between the lighter and heavier REEs is due to reduced precision in the

determination of less abundant elements, which is more pronounced for the basaltic horizons as trace element concentrations are lower in these shards compared to the rhyolitic horizons.

Average REE profiles for the rhyolitic horizons have broadly comparable patterns with a steep gradient for the LREEs (La–Nd), a distinct negative Eu anomaly and a relatively flat profile for the HREEs (Sm–Lu) (Fig. 8a). They all fall within the end-member characterisations envelope for Icelandic material (Fig. 8c). The Rb/Sr ratios for the rhyolitic horizons are comparable to those found in proximal Icelandic material (Fig. 8d), however, concentrations are lower for the distal material. The profile for LINK 16 675–680 cm differs slightly from the other two profiles with concentrations lower for the LREEs and higher for the HREEs (Fig. 8c). This can be attributed to LINK 16 675–680 cm deriving from an eruption in the Icelandic Rift Zone compared to the off-rift source of the other horizons (Table 3).
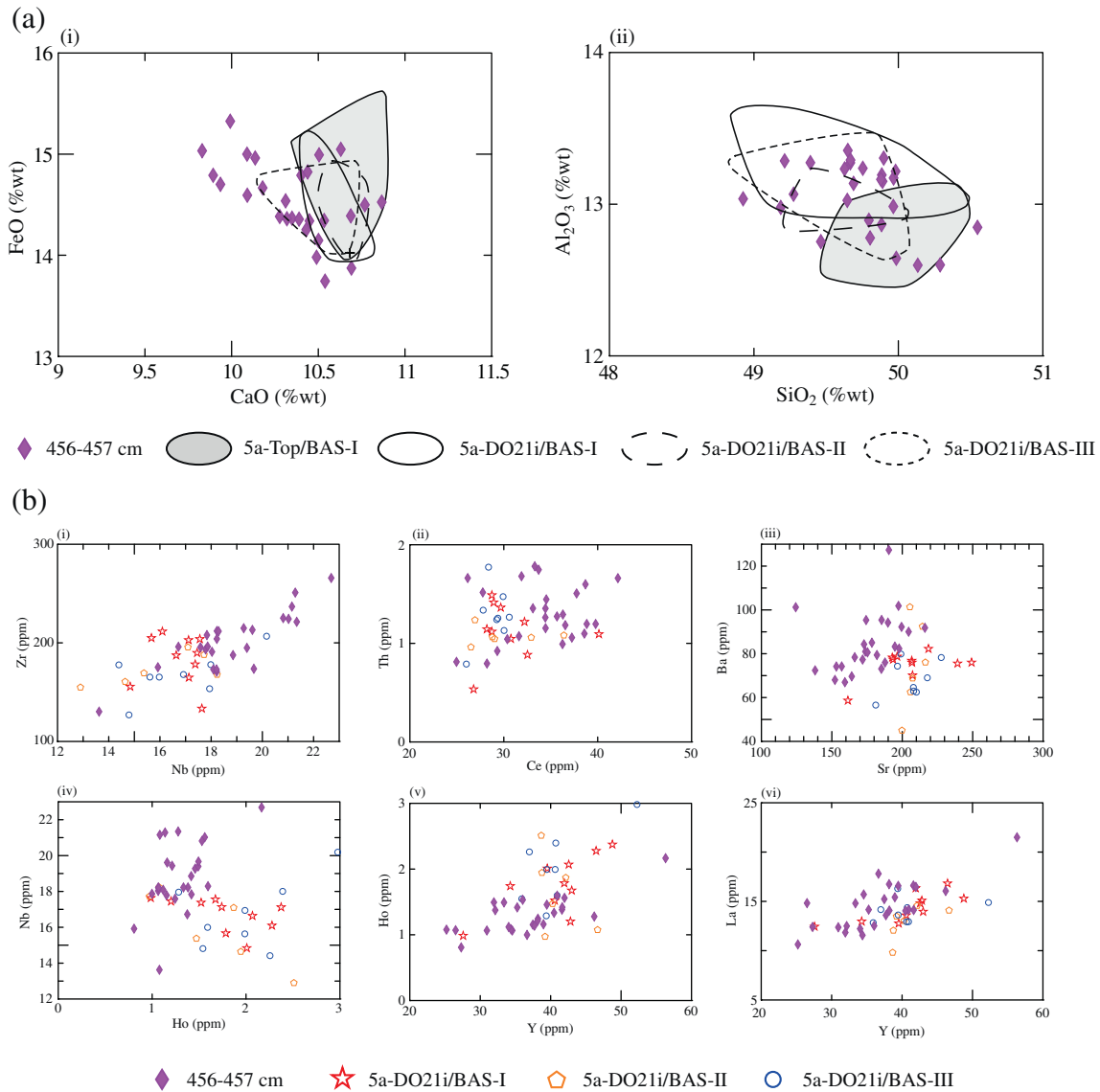
Fig. 6. (a) Comparison of the major element composition of the basaltic LINK 16 456–457 cm to MIS 5a basaltic horizons within MD95-2009 (5a-Top/BAS-I; Wastegård and Rasmussen, 2001) and MD99-2289 (5a-DO21i/BAS-I, -II, -III; Brendryen et al., 2010). (b) Comparisons of the trace element composition of the LINK 16 456–457 cm horizon and the 5a-DO21i/BAS-I, -II and -III horizons from Brendryen et al. (2010).

The average REE profiles for the three basaltic horizons are highly similar with all displaying a gentle gradient between La and Lu (Fig. 8c). The overall concentrations of the REEs exceed those of the proximal end-member characterisations for tholeiitic material presented in Óskarsson et al. (1982). However, it is unlikely that this is due to a source mis-attribution based on the major element analyses as the REE profiles are not as steep as those observed for more alkaline material (Fig. 8c) and the Rb and Sr concentrations for these tholeiitic deposits are highly similar to the characterisations of proximal tholeiitic material (Fig. 8d). The lower REE concentrations in the proximal deposits may be due to the bulk analyses used to gain these characterisations incorporating phenocrysts and lithic phases with lower REE concentrations than the juvenile glass analysed here using LA-ICP-MS.

3.6. Testing correlations using trace element compositions

In order to test two potential tephra correlations, new trace element data are presented from the Norwegian Sea core MD99-2289.

3.6.1. LINK 16 456–457 cm — MD99-2289 5a-DO21i-I, -II, -III

Trace element characterisation of the late MIS 5a basaltic horizons 5a-DO21i/BAS-I, -II, and -III from MD99-2289 re-affirms the major element results and confirms that they are geochemically indistinguishable (Fig. 6b). This may suggest that the ash zone represents reworking of material from a single eruptive episode or three closely spaced events, as suggested by Brendryen et al. (2010). In Section 3.4 a correlation between this deposit and LINK 16 456–457 cm was suggested, however, there are contrasts in trace element composition between the horizons, with overlapping but not consistent geochemical fields (Fig. 6b). These trace element differences can be attributed to differing levels of geochemical evolution, with fractional crystallisation occurring during evolution and between the eruption of the MD99-2289 deposit and the LINK 16 deposit. Fig. 6bi and ii shows that incompatible elements generally have higher concentrations in the LINK 16 deposit. These elements are not partitioned during evolution by fractional crystallisation so will have higher concentrations in more evolved magma, however, consistency in incompatible element ratios between the deposits suggests a genetic link between them. The lower Sr
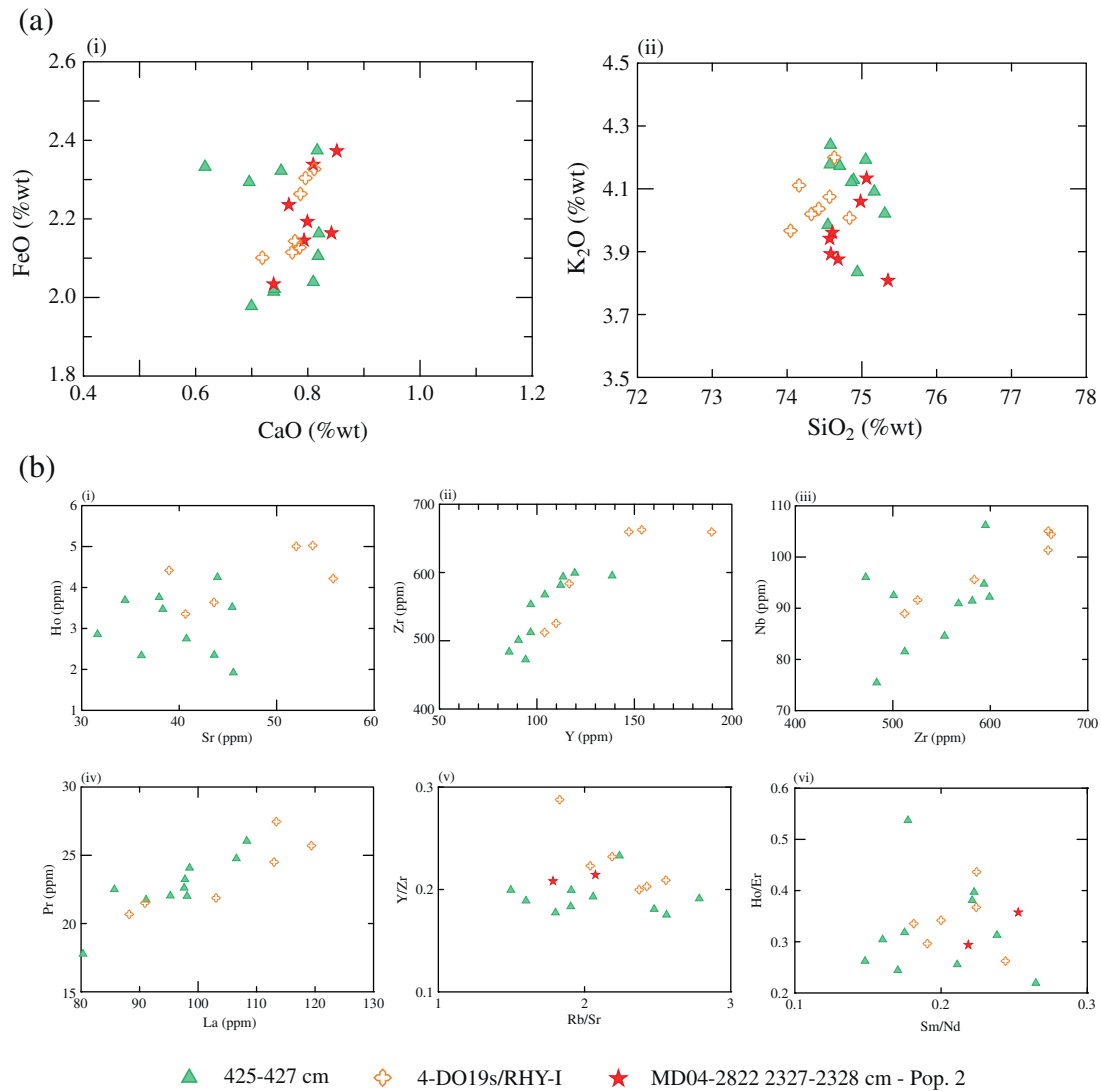
Fig. 7. (a) Comparison of the major element composition of the rhyolitic LINK 16 425–427 cm horizon to MIS 4 rhyolitic horizons within MD99-2289 (Brendryen et al., 2010) and MD04-2822 (Abbott et al., 2011, 2013). (b) Trace element comparisons of the composition of the LINK 16 425–427 cm horizon, the 4-DO19s/RHY-I horizon from Brendryen et al. (2010) and population 2 of MD04-2822 2327–2328 cm from Abbott et al. (2011).

concentrations (Fig. 6biii) and lower Y and Ho concentrations (Fig. 6bv and vi) in the LINK 16 material suggests that crystallisation of plagioclase and clinopyroxene has occurred as these compatible elements respectively partition into these minerals. Using the most abundant compatible and incompatible elements (Sr, Ba, Zr, Nb, Ce, Th) and the fractional crystallisation (FC) modelling spreadsheet "Petromodeller" from Ersoy (2013) it is possible to model the difference between the two average compositions by extracting approximately a 16% mixture of 65% plagioclase (using a Kd of Sr for plagioclase of 3, see GERM, 2013) and 35% clinopyroxene. This is consistent with subtle differences in the average major element chemistry between these samples. The MD99-2289 material has higher CaO, MgO, and Al_2O_3 and lower SiO_2, FeO, Na_2O, and K_2O concentrations than the LINK 16 material, which would be expected if the two were linked by fractionation of a cotectic mixture of plagioclase and pyroxene. Additionally a small decrease in P_2O_5 between MD99-2289 and LINK 16 implies a trace of apatite may have been removed, but an increase in TiO_2 implies that ilmenite crystallisation is not significant. Overall, this evolution could mean that the deposits were produced by two eruptions during DO-21 of the same volcanic system or two phases of the same eruption, the latter

implying a negligible temporal separation in the deposition of both of these horizons.

3.6.2. LINK 16 425–427 cm — MD99-2289 4-DO19s/RHY-I — MD04-2822 2327–2328 cm (population 2)

Trace element analysis of shards from the 4-DO19s/RHY-I horizon permitted a secondary comparison to LINK 16 425–427 cm and MD04-2822 2327–2328 cm (population 2) (Fig. 7b). Trace element data for MD04-2822 2327–2328 cm (population 2) from Abbott et al. (2011) was obtained prior to improved monitoring of gas blanks during the analysis of small shards using LA-ICP-MS (see Pearce et al., 2011), however as trace element ratios were unaffected by this methodological problem ratio/ratio comparisons can be made (Fig. 7bv and vi).

Bimodality is displayed in the trace element characterisations of the 4-DO19s/RHY-I material with three analyses plotting consistently within the envelope of the LINK 16 425–427 cm characterisation. The remaining three analyses, while falling outside the envelope for this material display similar ratio trends when both compatible and incompatible elements are compared (Fig. 7bi–iv). This could be due to the low number of shards analysed and thus the full compositional range
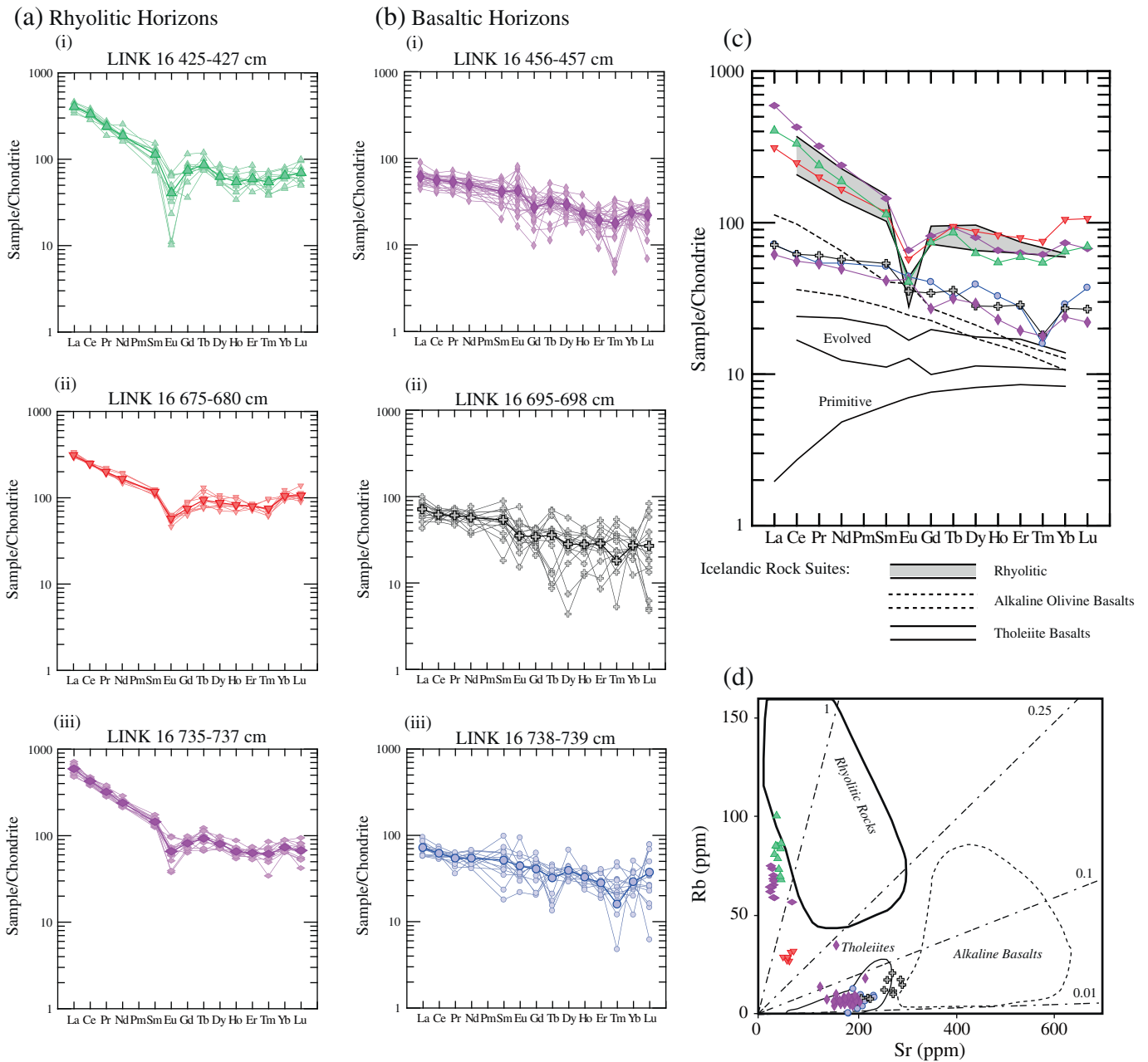
Fig. 8. Trace element characterisations of isochronous tephra horizons within LINK 16. (a) Chondrite-normalised REE profiles for individual shard analyses and average values (bold) for three rhyolitic horizons. (b) Chondrite-normalised REE profiles for individual shard analyses and average values (bold) for three basaltic horizons. Chondrite compositions from Sun and McDonough (1989). (c) Comparison of average chondrite-normalised REE profiles for the six LINK 16 horizons to REE patterns for Icelandic volcanic material (modified from Óskarsson et al., 1982). Analyses from O'Nions and Grönvold (1973) and O'Nions et al. (1973). (d) Sr vs. Rb compositional variation diagram comparing the individual analyses from the LINK 16 horizons to end-member characterisations defined by Óskarsson et al. (1982).

is not captured. Comparison of trace element ratios between the three deposits (Fig. 7bv and vi) demonstrates high consistency between the characterisations. Overall, the strong similarities and absence of evidence for fractional crystallisation demonstrates that the trace element results support and thus strengthen this correlation.

4. Discussion

4.1. Refining the Faroe Islands region tephrostratigraphy

Six tephra horizons have been identified in LINK 16 that have the potential to act as isochronous marker horizons (Table 3; Fig. 9). Three

deposits (LINK 16 456–457 cm, 675–680 cm and 695–697 cm) have been identified previously by Wastegård and Rasmussen (2001). The three cryptotephras added to the regional tephrostratigraphy (LINK 16 425–427 cm, 735–737 cm and 738–739 cm) resulted from extending investigations beyond MIS 5 into late MIS 6 and early MIS 4. The tephrostratigraphy of LINK 16 closely resembles the nearby MD95-2009 record with both displaying clear tephra shard peaks in contrast to the broad ash zones apparent within the ENAM33 record. Tracing these three common horizons between LINK 16 and MD95-2009 and their consistent stratigraphic positions helps to demonstrate that local, site-specific factors have not influenced deposition and stratigraphic integrity.

Table 3
Summary of MIS 6–4 tephra deposits identified in the LINK 16 sequence and correlations to previously identified MIS 6–4 tephra horizons.

Depth interval	Timing	Composition	Potential source	Transport pathway	Correlations	Potential widespread isochron?
425–427 cm	MIS 4	Transitional alkali rhyolitic	Öraefajökull or Torfajökull, Iceland	Primary airfall	MD04-2822 2327–2328 cm — pop. 2 4-DO19s/RHY-I	Yes
456–457 cm	MIS 5a	Tholeiitic basaltic	Grímsvötn, Iceland	Sea-ice rafting	5a-Top/BAS-I 5a-DO21i/BAS-I, II, III	Yes
485–486 cm	MIS 5a	Heterogeneous rhyolitic	Multiple Icelandic systems	Iceberg rafting	N/A	No
604–605 cm	MIS 5c	Heterogeneous tholeiitic basaltic	Multiple Icelandic Rift Zone systems	Iceberg rafting	5c-Midt/BAS-I 5c-DO24/BAS-I	No
675–680 cm	MIS 5e	Tholeiitic rhyolitic	Icelandic Rift Zone	Primary airfall	5e-Midt/RHY 5e-Eem/RHY-I	Yes
695–697 cm	MIS 5e	Tholeiitic basaltic	Grímsvötn, Iceland	Primary airfall	5e-Low/BAS-IV	Yes
735–737 cm	MIS 6	Transitional alkali rhyolitic	Öraefajökull or Torfajökull, Iceland	Primary airfall	New horizon	Yes
738–739 cm	MIS 6	Tholeiitic basaltic	Grímsvötn, Iceland	Primary airfall	New horizon	Yes

Thorough analysis of variations in tephra content between different grain-size fractions, co-variance with the IRD proxy and comprehensive geochemical characterisations permitted an assessment of depositional processes, thus aiding our classification of horizons as valuable isochrons. For example, a dominance of fine-grained material and lack of coeval IRD peaks indicates that five of the horizons were most likely deposited by primary airfall. In contrast, the identification of geochemical heterogeneity of shards from 485–486 cm and 604–605 cm indicates that these deposits were iceberg-rafted in origin and cannot be considered to be isochronous horizons. The comprehensive nature of the geochemical characterisations and the use of a proxy record for IRD demonstrates that LINK 16 604–605 cm was most likely deposited via iceberg rafting and thus cannot be used as a widespread isochronous horizon.

Few horizons deposited during this period have previously been analysed for trace elements, however, the secondary fingerprints presented in this study are a first step towards future comparisons and the testing of correlations as demonstrated in Section 3.6.

4.2. Synchronisation and correlation of palaeoclimatic archives during MIS 6–4

In addition to tracing horizons between the Faroe sequences tie-lines between more disparate archives have been defined and they have characteristics which could permit their use as key horizons for correlating records from this period (Fig. 9; Davies et al., in press). For instance, the correlation of LINK 16 675–680 cm to the 5e-Midt/RHY, the most widespread tephra horizon within this period (see Section 3.2), permits the correlation of this core to numerous records from the North Atlantic and the Klaksvík terrestrial sequence on the Faroe Islands (Wastegård et al., 2005; Table 1). Moreover, this study has also demonstrated the widespread nature of another rhyolitic horizon, the 4-DO19s/RHY-I, which can now be traced between the Norwegian Sea, the Faroe Islands region and the Rockall Trough and potentially has a proximal correlative in Iceland (Section 3.4). Based on the tuning of records to the Greenland ice-cores this provides a useful tie point for the initiation of cold conditions following DO(GI)-19 (Brendryen et al., 2010; Abbott et al., 2011; Davies et al., in press). This correlation, however, only became apparent after re-analysis of MD99-2289 material under the same microprobe conditions. The 'side-by-side' or repetition of analyses utilising the same conditions when testing potential correlations has been advocated previously, for example by Lowe (2011), Bourne et al. (2013) and Pearce et al. (2014). We also encourage that, when feasible, this approach be followed and recommend the importance of archiving samples for reanalysis.

The correlation of LINK 16 456–457 cm, to the 5a-Top/BAS-I of Wastegård and Rasmussen (2001), also represents a marker for the transition between MIS 5a and 4 (Fig. 2). The correlation of this deposit to the MD99-2289 sequence, however, highlights a complex scenario whereby it is difficult to determine whether the deposits are the products of two phases of one eruption or separate eruptive events (see Section 3.6.1). It is therefore recommended that any future tracing of this deposit acknowledges these differences and if possible trace element characterisations should be obtained from any potential correlative horizons and from multiple depths in dispersed deposits. This would allow the distribution of the different phases/eruptions to be mapped and the potential identification of material with both characterisations at a single site may help to resolve the temporal phasing of the eruptive processes.

The 5c-Midt/BAS-I horizon of Wastegård and Rasmussen (2001) was previously traced into the Norwegian Sea by Brendryen et al. (2010), 5c-DO24/BAS-I, and a population of LINK 16 604–605 cm relates to these deposits (Figs. 2 and 9). We have shown that it was most likely deposited at all the sites via iceberg rafting, which precludes its use as a widespread isochronous horizon but it is useful as a regional marine–marine tie-line and may help in the reconstruction of past ocean surface circulation (e.g. Kuhs et al., 2014). The heterogeneous geochemistry of LINK 16 604–605 cm provided strong support for transport via iceberg rafting, however, this characteristic was not identified in the earlier studies. It is possible that the acquisition of a larger number of major element analyses and the study of material down to 25 μm diameter in this study highlighted this complexity.

LINK 16 695–698 cm, correlated to the 5e-Low/BAS-IV in ENAM33 and MD95-2009, falls close to the start of the MIS 5e period and could be a key marker for this transition if it can be traced into other sequences. This deposit displayed the highest basaltic shard counts in all grain-size fractions throughout this core. Neither of the MIS 6 horizons identified in LINK 16 can be traced into other records, however, this could be attributed to a lack of focus on this period within previous tephrostratigraphical studies and both could provide tie-lines for the penultimate glacial period.

5. Conclusions

The application of density separation methods to the study of LINK 16 has demonstrated how the assessment of fine-grained material is useful for tracing cryptotephras within the marine realm. The high-resolution tephra shard concentration profiles, IRD proxy comparisons and comprehensive geochemical characterisations of deposits permitted an exploration of the transport and depositional processes responsible for their emplacement and six isochronous horizons have been defined. Such assessments are crucial for the use of tephra horizons as isochronous tie-lines for climatic correlation and synchronisation (Griggs et al., in press). The use of trace element characterisations to test potential correlations of widespread deposits demonstrated that, in some instances, this can strengthen correlations while in others chemical differences add complexity to assessing correlations as they could represent two different eruptions or may relate to magmatic processes. Increased integration of trace element characterisation within studies of Icelandic tephra is required to fully assess the wider
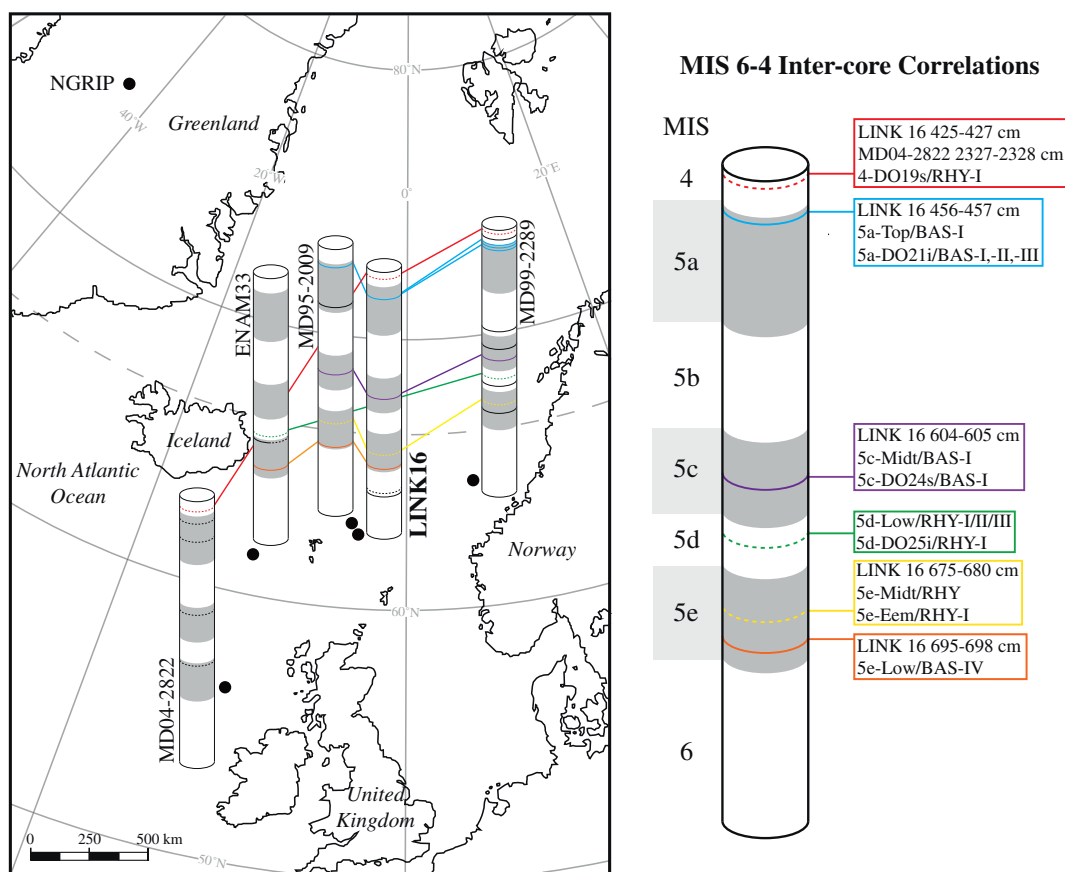
Fig. 9. (a) MIS 6–4 North Atlantic marine tephra horizons and correlations between five sequences. Coloured lines between records denote correlated horizons. Solid lines represent basaltic horizons and dashed lines denote rhyolitic horizons. MIS sub-stages in all cores have been scaled relative to the LINK 16 sequence. Details on tephra horizons from this work (LINK 16), Abbott et al. (2011, 2013) (MD04-2822), Wastegård and Rasmussen (2001) (ENAM 33 and MD95-2009) and Brendryen et al. (2010) (MD99-2289).

implications of this complexity and the utility of trace elements as a secondary test of distal correlations in the North Atlantic region.

All of the MIS 5 deposits identified within LINK 16 had been previously incorporated in the tephrostratigraphy for the Faroe Islands region by Wastegård and Rasmussen (2001). However, our reassessment with new techniques emphasised the isochronous nature of three horizons while highlighting how some deposits cannot be regarded as isochronous, such as the mid-MIS 5c deposit. Three isochronous horizons, a widespread MIS 4 rhyolitic horizon and two newly identified MIS 6 horizons, have been added to the regional tephrostratigraphy due to the extension of investigations to cover the MIS 4 and late MIS 6 periods. Overall, the six isochronous horizons are important components of the overall tephrostratigraphy of MIS 6–4 in the North Atlantic region (Davies et al., in press). The identification of such isochronous horizons is an important step for utilising tephrochronology for the correlation and synchronisation of records to help assess the relative timing of the pronounced millennial-scale climatic changes that occurred during this period.

Appendix A. Supplementary data

Supplementary data to this article can be found online at http://dx.doi.org/10.1016/j.palaeo.2014.05.004.

References

Abbott, P.M., Davies, S.M., Austin, W.E.N., Pearce, N.J.G., Hibbert, F.D., 2011. Identification of cryptotephra horizons in a North East Atlantic marine record spanning marine isotope stages 4 and 5a (~60,000–82,000 a b2k). Quat. Int. 246, 177–189.

Abbott, P.M., Davies, S.M., Steffensen, J.P., Pearce, N.J.G., Bigler, M., Johnsen, S.J., Seierstad, I. K., Svensson, A., Wastegård, S., 2012. A detailed framework of Marine Isotope Stage 4 and 5 volcanic events recorded in two Greenland ice-cores. Quat. Sci. Rev. 36, 59–77.

Abbott, P.M., Austin, W.E.N., Davies, S.M., Pearce, N.J.G., Hibbert, F.D., 2013. Cryptotephrochronology of a North East Atlantic marine sequence over Termination II, the Eemian and the last interglacial–glacial transition. J. Quat. Sci. 28, 501–514.

Austin, W.E.N., Hibbert, F.D., 2012. Tracing time in the ocean: a brief review of chronological constraints (60–8 kyr) on North Atlantic marine event-based stratigraphies. Quat. Sci. Rev. 36, 28–37.

Austin, W.E.N., Wilson, L.J., Hunt, J.B., 2004. The age and chronostratigraphical significance of North Atlantic Ash Zone II. J. Quat. Sci. 19, 137–146.

Blockley, S.P.E., Pyne-O'Donnell, S.D.F., Lowe, J.J., Matthews, I.P., Stone, A., Pollard, A.M., Turney, C.S.M., Molyneux, E.G., 2005. A new and less destructive laboratory procedure for the physical separation of distal glass tephra shards from sediments. Quat. Sci. Rev. 16–17, 1952–1960.

Bourne, A.J., Davies, S.M., Abbott, P.M., Rasmussen, S.O., Steffensen, J.P., Svensson, A., 2013. Revisiting the Faroe Marine Ash Zone III in two Greenland ice cores: implications for marine–ice correlations. J. Quat. Sci. 28, 641–646.

Brendryen, J., Haflidason, H., Sejrup, H.P., 2010. Norwegian Sea tephrostratigraphy of marine isotope stages 4 and 5: prospects and problems for tephrochronology in the North Atlantic region. Quat. Sci. Rev. 29, 847–864.

Brendryen, J., Haflidason, H., Sejrup, H.P., 2011. Non-synchronous deposition of North Atlantic Ash Zone II in Greenland ice cores, and North Atlantic and Norwegian Sea sediments: an example of complex glacial-stage tephra transport. J. Quat. Sci. 26, 739–745.

Capron, E., Landais, A., Chappellaz, J., Schilt, A., Buiron, D., Dahl-Jensen, D., Johnsen, S.J., Jouzel, J., Lemieux-Dudon, B., Loulergue, L., Leuenberger, M., Masson-Delmotte, V., Meyer, H., Oerter, H., Stenni, B., 2010. Millennial and sub-millennial scale climate variations recorded in polar ice cores over the last glacial period. Clim. Past 6, 345–365.

Davies, S.M., Hoek, W.Z., Bohncke, J.P., Lowe, J.J., Pyne-O'Donnell, S., Turney, C.S.M., 2005. Detection of Lateglacial distal tephra layers in the Netherlands. Boreas 34, 123–135.

Davies, S.M., Abbott, P.M., Meara, Rh., Pearce, N.J.G., Austin, W.E.N., Chapman, M.R., Svensson, A., Bigler, M., Rasmussen, T.L., Rasmussen, S.O., 2014. A North Atlantic tephra framework for 130–60 ka b2k: new tephra discoveries, marine based-correlations and future challenges. Quat. Sci. Rev. (in press).

Ersoy, E.Y., 2013. "PETROMODELER" (Petrological Modeler): a Microsoft Excel spreadsheet program for modelling melting, mixing, crystallization and assimilation processes in magmatic systems. Turk. J. Earth Sci. 22, 115–125.

Fronval, T., Jansen, E., 1997. Eemian and early Weichselian (140–160 ka) paleoceanography and paleoclimate in the Nordic seas with comparisons to Holocene conditions. Paleoceanography 12, 443–462.

Fronval, T., Jansen, E., Haflidason, H., Sejrup, H.P., 1998. Variability in surface and deep water conditions in the Nordic Seas during the Last Interglacial Period. Quat. Sci. Rev. 17, 963–985.

GERM, 2013. Geochemical Earth Reference Model (GERM) Partition Coefficient (Kd) Database. www.earthref.org/KDD/.

Griggs, A.J., Davies, S.M., Abbott, P.M., Rasmussen, T.L., Palmer, A.P., 2014. Optimising the use of marine tephrochronology in the North Atlantic: a detailed investigation of the Faroe Marine Ash Zones II, III and IV. Quat. Sci. Rev. (in press).

Gudmundsdóttir, E.R., Eiríksson, J., Larsen, G., 2011. Identification and definition of primary and reworked tephra in Late Glacial and Holocene marine shelf sediments off North Iceland. J. Quat. Sci. 26, 589–602.

Haflidason, H., Eiríksson, J., Van Kreveld, S., 2000. The tephrochronology of Iceland and the North Atlantic region during the Middle and Late Quaternary: a review. J. Quat. Sci. 15, 3–22.

Hayward, C., 2012. High spatial resolution electron probe microanalysis of tephras and melt inclusions without beam-induced chemical modification. The Holocene 119–125.

Höskuldsson, Á., Sparks, R.S.J., Carroll, M.R., 2006. Constraints on the dynamics of subglacial basalt eruptions from geological and geochemical observations at Kverkfjöll, NE-Iceland. Bull. Volcanol. 68, 689–701.

Jakobsson, S.P., 1979. Petrology of recent basalts of the Eastern Volcanic Zone, Iceland. Acta Nat. Island. 26, 1–103.

Jakobsson, S.P., Jónasson, K., Sigurdsson, I.A., 2008. The three igneous rock suites of Iceland. Jökull 58, 117–138.

Jónasson, K., 2007. Silicic volcanism in Iceland: composition and distribution within the active volcanic zones. J. Geodyn. 43, 101–117.

Kuhs, M., Austin, W.E.N., Abbott, P.M., Hodell, D.A., 2014. Iceberg-rafted tephra as a potential tool for the reconstruction of ice-sheet processes and ocean surface circulation in the glacial North Atlantic. In: Austin, W.E.N., Abbott, P.M., Davies, S.M., Pearce, N.J.G., Wastegård, S. (Eds.), Marine Tephrochronology. Geological Society of London Special Publication, 398.

Lacasse, C., Garbe-Schönberg, C.-D., 2001. Explosive silicic volcanism in Iceland and the Jan Mayen area during the last 6 Ma: sources and timing of major eruptions. J. Volcanol. Geotherm. Res. 107, 113–147.

Le Maitre, R.W., Bateman, P., Dudek, A., Keller, J., Lameyre, Le Bas, M.J., Sabine, P.A., Schmid, R., Sorensen, H., Streckeisen, A., Woolley, A.R., Zanettin, B., 1989. A Classification of Igneous Rocks and Glossary of Terms. Blackwell, Oxford.

Lowe, D.J., 2011. Tephrochronology and its application: a review. Quat. Geochronol. 6, 107–153.

MacDonald, G.A., Katsura, T., 1964. Chemical composition of Hawaiian lavas. J. Petrol. 5, 83–133.

McGarvie, D.W., Burgess, R., Tindle, A.G., Tuffen, H., Stevenson, J.A., 2006. Pleistocene rhyolitic volcanism at Torfajökull, Iceland: eruption ages, glaciovolcanism and geochemical evolution. Jökull 56, 57–75.

McManus, J.F., Oppo, D.W., Keigwin, L.D., Cullen, J.L., Bond, G.C., 2002. Thermohaline circulation and prolonged interglacial warmth in the North Atlantic. Quat. Res. 58, 17–21.

Nielsen, T., Rasmussen, T.L., Ceramicola, S., Kuijpers, A., 2007. Quaternary sedimentation, margin architecture and ocean circulation variability around the Faroe Islands, North Atlantic. Quat. Sci. Rev. 26, 1016–1036.

North Greenland Ice Core Project Members, 2004. High-resolution record of Northern Hemisphere climate extending into the last interglacial period. Nature 431, 147–151.

Óladóttir, B.A., Sigmarsson, O., Larsen, G., Devidal, J.-L., 2011. Provenance of basaltic tephra from Vatnajökull volcanoes, Iceland, as determined by major- and trace-element analyses. The Holocene 21, 1037–1048.

O'Nions, R.K., Grönvold, K., 1973. Petrogenetic relationships of acid and basic rocks in Iceland: Sr-isotopes and rare-earth elements in late and postglacial volcanics. Earth Planet. Sci. Lett. 19, 397–409.

O'Nions, R.K., Pankhurst, R.J., Fridleifsson, I.B., Jakobsson, S.P., 1973. Strontium isotopes and rare earth elements in basalts from the Heimaey and Surtsey volcanic eruptions. Nature 243, 213–214.

Oppo, D.W., Horowitz, M., Lehman, S.J., 1997. Marine core evidence for reduced deep water production during Termination II followed by a relatively stable substage 5e (Eemian). Paleoceanography 12, 51–63.

Oppo, D.W., Keigwin, L.D., McManus, J.F., Cullen, J.L., 2001. Persistent suborbital climate variability in marine isotope stage 5 and Termination II. Paleoceanography 16, 280–292.

Óskarsson, N., Sigvaldason, G.E., Steinthórsson, S., 1982. A dynamic model of rift zone petrogenesis and the regional petrology of Iceland. J. Petrol. 23, 28–74.

Owen, J., Tuffen, H., McGarvie, D.W., 2013. Explosive subglacial rhyolitic eruptions in Iceland are fuelled by high magmatic H_2O and closed-system degassing. Geology 41, 251–254.

Pearce, N.J.G., Denton, J.S., Perkins, W.T., Westgate, J.A., Alloway, B.V., 2007. Correlation and characterisation of individual glass shards from tephra deposits using trace element laser ablation ICP-MS analyses: current status and future potential. J. Quat. Sci. 22, 721–736.

Pearce, N.J.G., Perkins, W.T., Westgate, J.A., Wade, S.C., 2011. Trace-element microanalysis by LA-ICP-MS: the quest for comprehensive chemical characterisation of single, sub-10 μm volcanic glass shards. Quat. Int. 246, 57–81.

Pearce, N.J.G., Abbott, P.M., Martin-Jones, C., 2014. Microbeam methods for the analysis of glass in fine grained tephra deposits: a SMART perspective on current and future trends. In: Austin, W.E.N., Abbott, P.M., Davies, S.M., Pearce, N.J.G., Wastegård, S. (Eds.), Marine Tephrochronology. Geological Society of London Special Publication, 398.

Rasmussen, T.L., Thomsen, E., 2009. Ventilation changes in intermediate water on millennial time scales in the SE Nordic seas, 65–14 kyr BP. Geophys. Res. Lett. 36. http://dx.doi.org/10.1029/2008GL036563.

Rasmussen, T.L., Thomsen, E., van Weering, T.C.E., Labeyrie, L., 1996. Rapid changes in surface and deep water conditions at the Faeroe Margin during the last 58,000 years. Paleoceanography 11, 757–771.

Rasmussen, T.L., Balbon, E., Thomsen, E., Labeyrie, L., van Weering, T.C.E., 1999. Climate records and changes in deep outflow from the Norwegian Sea ~150–55 ka. Terra Nova 11, 61–66.

Rasmussen, T.L., Wastegård, S., Kuijpers, A., van Weering, T.C.E., Heinemeier, J., Thomson, E., 2003. Stratigraphy and distribution of tephra layers in marine sediment cores from the Faeroe Islands, North Atlantic. Mar. Geol. 199, 263–277.

Sejrup, H.P., Sjøholm, J., Furnes, H., Beyer, I., Eide, L., Jansen, E., Mangerud, J., 1989. Quaternary tephrochronology on the Iceland Pleateau, north of Iceland. J. Quat. Sci. 4, 109–114.

Sjøholm, J., Sejrup, H.P., Furnes, H., 1991. Quaternary volcanic ash zones on the Iceland Plateau, southern Norwegian Sea. J. Quat. Sci. 6, 159–173.

Sun, S.S., McDonough, W.F., 1989. Chemical and isotopic systems of oceanic basalts: implications for mantle composition and processes. In: Saunders, A.D., Norry, M.J. (Eds.), Magmatism in Ocean Basins. Geol. Soc. London Spec. Pub., 42, pp. 313–345.

Todd, J.A., Austin, W.E.N., Abbott, P.M., 2014. Quantifying bioturbation of a simulated ash fall event. In: Austin, W.E.N., Abbott, P.M., Davies, S.M., Pearce, N.J.G., Wastegård, S. (Eds.), Marine Tephrochronology. Geological Society of London Special Publication, 398.

Turney, C.S.M., 1998. Extraction of rhyolitic ash from minerogenic lake sediments. J. Paleolimnol. 19, 199–206.

Wastegård, S., Rasmussen, T.L., 2001. New tephra horizons from Oxygen Isotope 5 in the North Atlantic: correlation potential for terrestrial, marine and ice-core archives. Quat. Sci. Rev. 20, 1587–1589.

Wastegård, S., Björck, S., Greve, C., Rasmussen, T.L., 2005. A tephra-based correlation between the Faroe Islands and the Norwegian Sea raises questions about chronological relationships during the last interglacial. Terra Nova 17, 7–12.